Systematic study of the transverse flow and its disappearance: Role of nuclear compressibility and momentum-dependent interactions

Rajni Bansal[1] and Sakshi Gautam[2,*]

[1]*Department of Physics, Mehr Chand Mahajan D. A. V. College for Women, Sector 36 A, Chandigarh 160 036, India*

[2]*Department of Physics, Panjab University, Chandigarh 160 014, India*

(Received 2 March 2014; revised manuscript received 31 January 2015; published 23 February 2015)

We investigate the energy of vanishing flow (EVF) as a function of colliding geometry for various reactions and confront our theoretical calculations with available experimental data. Our findings using an isospin-dependent quantum molecular dynamics (IQMD) model reveal that measured energies of vanishing flow can be reproduced nicely by IQMD model calculations. We also analyze, in detail, the role of hard and soft equations of state (with and without momentum-dependent interactions) in transverse flow and its disappearance over a wide range of mass and impact parameters. Our investigations reveal that the mass dependence of the energy of vanishing flow at peripheral collisions can act as a useful probe to pin down the stiffness of nuclear matter.

DOI: 10.1103/PhysRevC.91.024615 PACS number(s): 25.75.Ld, 24.10.Cn, 21.65.Cd, 24.10.Lx

I. INTRODUCTION

The studies on collective flow in heavy-ion reactions still interest the nuclear physics community because they provide information about the hot and dense nuclear matter formed during a collision [1–5]. This observable is found to be one of the best candidates among others such as fragmentation [6], nuclear stopping [7], and strangeness production at threshold energies [8] used to probe the nuclear equation of state (EOS). The energy dependence of the collective flow leads to its disappearance at a particular incident energy because of the interplay between the attractive mean field (dominant at lower incident energies) and repulsive nucleon-nucleon (*nn*) scattering (dominant at higher incident energies) [9]. The energy of disappearance of flow is also termed as the energy of vanishing flow (EVF) or balance energy. This energy is found to be free from the reaction plane determination and thus theoretical results can be directly compared with the measured ones.

The EVF has been reported to be sensitive towards various properties of nuclear matter: nuclear EOS [10–14] and in-medium *nn* cross sections [14–16], system mass [10,13,14,17,18], colliding geometry [12,13,19–24], isospin [21,22,24], and mass asymmetry of the reacting partners [25]. The energies of vanishing flow have been measured experimentally for more than a dozen reactions ranging between $^{12}C + ^{12}C$ and $^{197}Au + ^{197}Au$. Interestingly, most of these measurements have been constrained to central collisions only [9,10,12,16,19–21,26–31]. Few investigations, however, also included peripheral collisions [12,16,19–21,27–29]. Among these one has the reactions $^{36}Ar + ^{27}Al$ [27,28], $^{40}Ar + ^{27}Al$ [29], $^{40}Ar + ^{45}Sc$ [19], $^{64}Zn + ^{27}Al$ [16], $^{58}Ni + ^{58}Ni$ [12,20,21], $^{58}Fe + ^{58}Fe$ [20,21], $^{64}Zn + ^{48}Ti$ [28], $^{64}Zn + ^{58}Ni$ [27,28], $^{86}Kr + ^{93}Nb$ [12], and $^{197}Au + ^{197}Au$ [12]. Similar efforts have also been carried out theoretically for central and peripheral geometries [12,19,22,23,32]. Unfortunately, these efforts were either limited to narrow mass range or colliding geometry was restricted. For example, in Ref. [32], the EVF for the reaction $^{40}Ca + ^{40}Ca$ was reported as a function of impact parameter using quantum molecular dynamics (QMD) calculations. In Ref. [16], Boltzmann-Uehling-Uhlenbeck (BUU) model predictions of EVF were reported for semicentral and peripheral collisions of $^{64}Zn + ^{27}Al$ using different cross sections and EOS. The role of the isospin degree of freedom was analyzed in the reactions $^{58}Ni + ^{58}Ni$ and $^{58}Fe + ^{58}Fe$ using isospin Boltzmann-Uehling-Uhlenbeck (IBUU) [21], improved quantum molecular dynamics (ImQMD) [33], and isospin-dependent quantum molecular dynamics (IQMD) [22] models. Recently, Kaur *et al.* [34] compared their IQMD calculations of EVF for the reactions $^{40}Ar + ^{45}Sc$, $^{58}Ni + ^{58}Ni$, $^{86}Kr + ^{93}Nb$, and $^{197}Au + ^{197}Au$ with the measured data as a function of impact parameter. We also reported the calculations of EVF for the central collisions of various reactions ranging between $^{12}C + ^{12}C$ and $^{197}Au + ^{197}Au$ [35]. In this study, a soft momentum-dependent interaction along with a 20% reduction in the cross section was found to reproduce the data precisely. Further, it has also been shown in Ref. [35] that once the physical parameters are fixed, various theoretical models yield nearly the same EVF in most cases. A careful analysis of the literature leads to following conclusions: (i) most of the theoretical attempts are limited to central collisions only and (ii) there are several contradictory results reported with respect to different EOS and their momentum dependence as well as to cross sections [2,9,11–13,15–18,36]. Interestingly, most of these combinations can reproduce one or the other aspects of experimental data. For example, in Ref. [36] soft EOS lead to higher EVF throughout the mass range compared to hard EOS, contrary to the predictions of Refs. [9,15], where hard EOS were reported to have higher EVF. The sensitivity of EVF towards different EOS was also found to depend on the size of colliding nuclei [11,13] as well as on the momentum dependence of the mean field [14,17].

From the above survey it is evident that a complete systematic study is still missing in the literature. Therefore, our present aim is at least twofold: (i) to confront experimental measurements of impact parameter dependence of EVF over a

*sakshigautam@pu.ac.in

wider mass range with theoretical calculations and (ii) to study the role of model ingredients such as nuclear compressibility and momentum-dependent interactions on transverse flow for central and peripheral collisions and to present a unified picture of their role. The present study is carried out within the framework of an IQMD model, which is discussed briefly in Sec. II. The results are discussed in Sec. III and a summary is given in Sec. IV.

II. THE MODEL

The IQMD model explicitly includes the isospin degree of freedom [37]. The IQMD model treats different charge states of nucleons, deltas, and pions explicitly. The IQMD model has been used successfully for the analysis of a large number of observables from low to relativistic energies [22,24,35,38–41]. The isospin degree of freedom enters into the calculations via symmetry potential, cross sections, and Coulomb interaction. Here we use the experimental *nn* cross section with explicit isospin dependence. In this model, successfully initialized projectile and target nuclei that fulfil structural constraints such as the binding energy, the root-mean-square radius, and the density profile are boosted towards each other with proper center-of-mass velocity using relativistic kinematics. Here each nucleon propagates using the classical equations of motion under the nuclear mean field parameterized as

$$\begin{aligned} V_{ij}(\vec{r}_i - \vec{r}_j) &= V_{ij}^{\text{Sky}} + V_{ij}^{\text{Yuk}} + V_{ij}^{\text{Coul}} + V_{ij}^{\text{MDI}} + V_{ij}^{\text{Sym}} \\ &= \Bigg[t_1 \delta(\vec{r}_i - \vec{r}_j) + t_2 \delta(\vec{r}_i - \vec{r}_j) \rho^{\gamma - 1} \\ &\quad \times \left(\frac{\vec{r}_i + \vec{r}_j}{2} \right) \Bigg] + t_3 \frac{\exp(|-(\vec{r}_i - \vec{r}_j)|/\mu)}{(|(\vec{r}_i - \vec{r}_j)|/\mu)} \\ &\quad + \frac{Z_i Z_j e^2}{|(\vec{r}_i - \vec{r}_j)|} + t_4 \ln^2(t_5(\vec{p}_i - \vec{p}_j)^2 + 1) \\ &\quad \times \delta(\vec{r}_i - \vec{r}_j) + t_6 \frac{1}{\rho_0} T_{3i} T_{3j} \delta(\vec{r}_i - \vec{r}_j). \end{aligned} \quad (1)$$

Here Z_i and Z_j denote the charges of the ith and jth baryons, and T_{3i} and T_{3j} are their respective T_3 components (i.e., $1/2$ for protons and $-1/2$ for neutrons). The parameters $t_1, \ldots, t_5$ are adjusted to the real part of the nucleonic optical potential.

III. RESULTS AND DISCUSSION

For the first part, we simulated the reactions ^{36}Ar + ^{27}Al, ^{40}Ar + ^{27}Al, ^{40}Ar + ^{45}Sc, ^{64}Zn + ^{27}Al, ^{58}Ni + ^{58}Ni, ^{58}Fe + ^{58}Fe, ^{64}Zn + ^{48}Ti, ^{64}Zn + ^{58}Ni, ^{86}Kr + ^{93}Nb, and ^{197}Au + ^{197}Au, whose experimental EVF at different impact parameters are available. The above reactions are simulated at different incident energies ranging between 40 and 400 MeV/nucleon at a step of 20 MeV/nucleon. A straight line interpolation is employed to find out the EVF in the energy range where directed transverse momentum changes sign from positive to negative values (i.e., crosses zero). We use a soft EOS with momentum-dependent interactions (MDI) along with a 20% reduced *nn* cross section throughout the article until specified otherwise. This choice of EOS and *nn* cross section is motivated by our previous study [35].

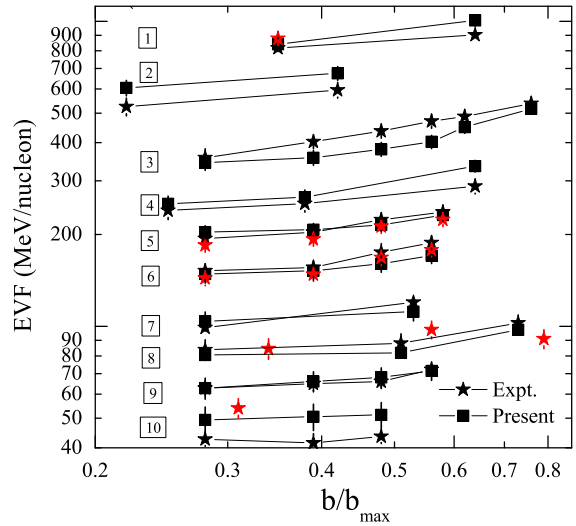

FIG. 1. (Color online) The energy of vanishing flow as a function of impact parameter (plotted at the upper limit of each bin). Stars represent experimental measurements whereas squares correspond to present calculations using SMD EOS with reduced *nn* cross sections. Lines are included to guide the eye. The curves tagged by 1–10 correspond to the reactions ^{36}Ar + ^{27}Al, ^{40}Ar + ^{27}Al, ^{40}Ar + ^{45}Sc, ^{64}Zn + ^{27}Al, ^{58}Ni + ^{58}Ni, ^{58}Fe + ^{58}Fe, ^{64}Zn + ^{48}Ti, ^{64}Zn + ^{58}Ni, ^{86}Kr + ^{93}Nb, and ^{197}Au + ^{197}Au, respectively, and the EVF for the above reactions has been scaled by a factor of 9.5, 7.0, 4.2, 3.2, 2.8, 2.0, 1.5, 1.3, 1.1, and 1.0, respectively.

In Fig. 1, we display the EVF as a function of impact parameter for all the above reactions. Stars (with error bars) represent measured energies of vanishing flow and squares correspond to our theoretical calculations. The EVF for various reactions have been rescaled by different factors to maintain the clarity of the figure. The experimental and theoretical EVF for the reactions of ^{36}Ar + ^{27}Al, ^{40}Ar + ^{27}Al, ^{40}Ar + ^{45}Sc, ^{64}Zn + ^{27}Al, ^{58}Ni + ^{58}Ni, ^{58}Fe + ^{58}Fe, ^{64}Zn + ^{48}Ti, ^{64}Zn + ^{58}Ni, ^{86}Kr + ^{93}Nb, and ^{197}Au + ^{197}Au have been scaled by a factor of 9.5, 7.0, 4.2, 3.2, 2.8, 2.0, 1.5, 1.3, 1.1, and 1.0, respectively. From the figure, we notice that the EVF rises as one moves from central to peripheral collisions. This dependence gets weaker for heavier systems. Our theoretical calculations are able to reproduce measured EVF reasonably in most of the cases. Further, the general trends of the EVF with mass and impact parameter are also reproduced. Here it is worth mentioning that in many cases there is a significant difference in the values of the EVF reported by various experimental groups. So, one can talk of general trends only. For example in Ref. [26], the measured EVF for the reaction ^{197}Au + ^{197}Au is around 60 MeV/nucleon in contradiction to earlier observation, where the EVF was estimated to be around 42 ± 4 MeV/nucleon [31].

For the second part of the article, we perform a controlled study. In this study, the isospin factor ($\frac{N-Z}{Z}$%) is kept nearly the same (i.e., ranging between 40% and 50%) for all the colliding pairs. The Gaussian width is also adjusted by a small amount so that the mass dependence of the EVF with soft momentum-dependent (SMD) EOS along with a 20% reduction in cross section gives the perfect dependence $\propto A^{-\tau}$.

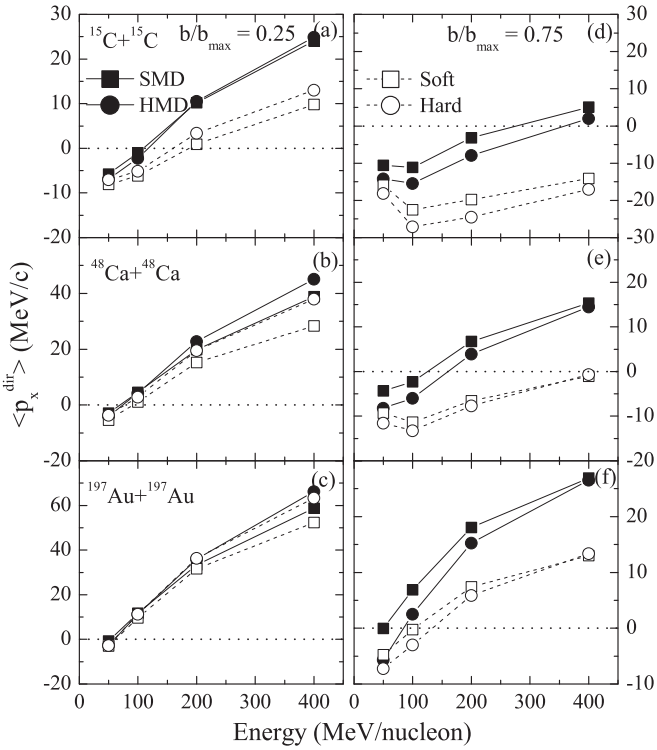

FIG. 2. The directed transverse momentum ($\langle p_x^{\rm dir}\rangle$) as a function of incident energy for central (left-hand panels) and peripheral (right-hand panels) collisions. Lines are included to guide the eye. Different symbols correspond to different equations of state as explained in the text.

Here we simulated the reactions $^{15}C + ^{15}C$, $^{24}Ne + ^{24}Ne$, $^{36}P + ^{36}P$, $^{48}Ca + ^{48}Ca$, $^{72}Zn + ^{72}Zn$, $^{96}Zr + ^{96}Zr$, $^{139}La + ^{139}La$, and $^{197}Au + ^{197}Au$ at $b/b_{\rm max} = 0.25$ and 0.75 (where $b_{\rm max} = A_P + A_T$; $A_{P/T}$ = mass of projectile/target nucleus).

It is worth mentioning that we have also simulated the reactions ranging between $^{12}C + ^{12}C$ and $^{197}Au + ^{197}Au$ whose experimental and/or measured EVF are available. Because these reactions were having varying isospin contents and measurements were carried out at different colliding geometries, we did not get absolute power-law dependence of EVF with system mass (A) (results not shown here). Therefore, for the systematic study of the mass dependence of EVF, it is absolutely necessary to constrain both the colliding geometry and the isospin content of the reactions and thus we restrict to the earlier-mentioned colliding pairs.

In Fig. 2, we display the directed transverse momentum ($\langle p_x^{\rm dir}\rangle$) as a function of incident energy for the reactions $^{15}C + ^{15}C$ (upper panels), $^{48}Ca + ^{48}Ca$ (middle panels), and $^{197}Au + ^{197}Au$ (lower panels) at both central (left-hand panels) and peripheral (right-hand panels) geometries. The solid (open) symbols represent the calculations with (without) momentum-dependent interactions. From the figure, we see that $\langle p_x^{\rm dir}\rangle$ increases with incident energy, for both static and momentum-dependent EOS as reported in earlier studies [15–18].

Let us first discuss central collisions [Figs. 2(a)–2(c)]. Here static hard EOS lead to higher $\langle p_x^{\rm dir}\rangle$ compared to soft EOS consistently. This is due to the fact that hard EOS are more repulsive compared to soft EOS. Also, the $\langle p_x^{\rm dir}\rangle$ is almost same with hard and soft EOS for all reactions at 50 MeV/nucleon. This is because of reduced excitation of nuclear matter at such a low incident energy and thus different compressibilities will yield the same directed transverse momentum. The sensitivity to different EOS, however, increases at higher incident energies. This is because of the significant difference in the nuclear compressibilities at higher densities (achieved at higher beam energies). An enhanced $\langle p_x^{\rm dir}\rangle$ is obtained with the inclusion of momentum-dependent interactions because of their repulsive nature. It should be noted that the inclusion of MDI also reduces the nuclear density (due to its repulsive character) and this, in turn, will lessen the number of binary *nn* collisions, which otherwise should result in less directed transverse momentum. The repulsive nature of MDI (enters into the mean-field contribution to $\langle p_x^{\rm dir}\rangle$) enhances the $\langle p_x^{\rm dir}\rangle$ far more than the reduction due to reduced binary collisions. We also noted that the increase in $\langle p_x^{\rm dir}\rangle$ due to MDI at higher energies is more pronounced for lighter systems compared to heavier ones. This may happen because of significant number of collisions in heavier systems which gets reduced due to repulsive MDI and thus the collision contribution to the total $\langle p_x^{\rm dir}\rangle$ is also reduced. This, in turn, will lessen the overall enhancement in the total $\langle p_x^{\rm dir}\rangle$ due to momentum dependence of the mean field. Therefore, the $\langle p_x^{\rm dir}\rangle$ for the heavier systems even with MDI does not change much with respect to that observed with static EOS.

It is interesting to note that the directed transverse momentum is almost same with soft and hard EOS when MDI are included throughout the energy range for the reaction $^{15}C + ^{15}C$. On the other hand, differences start appearing for the heavier masses at high energies. This is because of the fact that, when MDI are included, lower densities are achieved (because of these repulsive interactions) in the reactions involving lighter nuclei (such as $^{15}C + ^{15}C$) that lead to the same results with different EOS. On the other hand, for heavier systems, higher densities are achieved (even with MDI) at high incident energies and thus lead to different $\langle p_x^{\rm dir}\rangle$ with hard momentum-dependent (HMD) and SMD EOS.

Let us now discuss peripheral collisions [Figs. 2(d)–2(f)]. Here also directed transverse momentum is lower for static EOS compared to that involving MDI but the difference is much more pronounced compared to central collisions. A large number of binary collisions at central colliding geometry lowers the initial relative momentum between the nucleons, which reduces the influence of the momentum-dependent interactions. On the other hand, due to decreased compressional effects at peripheral collisions, nucleons feel stronger repulsion due to MDI in the initial phase of the reaction, which leads to enhanced sensitivity of the $\langle p_x^{\rm dir}\rangle$ towards MDI at peripheral colliding geometries. Similar conclusions have also been reported in earlier studies [32,42] where MDI were found to play a dominant role in peripheral collisions. Here, soft (SMD) EOS lead to more $\langle p_x^{\rm dir}\rangle$ compared to hard (HMD) EOS in contrast to earlier observations at the central collisions. To check this, we decomposed the directed transverse momentum into the contributions from the mean-field and two-body collisions. The mean-field contribution of hard and soft EOS

to the $\langle p_x^{\rm dir}\rangle$ (in peripheral collisions) is almost same because of the reduced densities. On the other hand, a soft EOS results in a greater collision contribution to the $\langle p_x^{\rm dir}\rangle$ compared to a hard EOS and thus one gets a higher directed transverse momentum in the former case. Moreover, the sensitivity of the $\langle p_x^{\rm dir}\rangle$ towards different EOS, i.e., hard or soft (either with or without MDI), decreases as one moves to higher incident energies. This is also contrary to the central collisions where enhanced sensitivity is observed at higher energies [as seen in Figs. 2(a)–2(c)]. In peripheral collisions at higher incident energies, hard and soft EOS result in almost the same mean field and collision contributions to the $\langle p_x^{\rm dir}\rangle$ and hence result in the same total $\langle p_x^{\rm dir}\rangle$. On the other hand, in central collisions at higher energies, hard EOS yield greater mean-field contributions to the $\langle p_x^{\rm dir}\rangle$ compared to soft EOS (whereas the collision contribution remains the same for both equations of state). Similar conclusions were also reported in Ref. [43], where the central collisions of ^{139}La + ^{139}La were studied at 800 MeV/nucleon. This, in turn, results in enhanced sensitivity of the $\langle p_x^{\rm dir}\rangle$ to the EOS at higher energies for central collisions. Similarly, sensitivity of the $\langle p_x^{\rm dir}\rangle$ towards different EOS with the inclusion of momentum-dependent interactions also decreases with energy. This is due to the much dominant role of MDI at peripheral colliding geometries and which further enhances at higher incident energies and, in turn, leads to much reduced densities and thus the role of different compressibilities almost disappears at higher energies. In addition, the $\langle p_x^{\rm dir}\rangle$ changes from negative to positive value at higher incident energies for lighter reactions, whereas this transition happens at lower incident energies for the reactions of heavy nuclei. The energy where $\langle p_x^{\rm dir}\rangle$ crosses zero (termed as the energy of vanishing flow) is higher at peripheral collisions as reported in earlier studies also [12,21–24].

In Fig. 3, we display the EVF as a function of total reacting mass (A) for central collisions (upper panels). The solid and open squares (circles) represent the calculations for the soft (hard) EOS, with and without MDI, respectively. The corresponding error bars have also been added. The left (right) panels display the results with (without) MDI interactions. From Fig. 3(a), we see that the EVF follows a power-law behavior ($\propto A^{-\tau}$) with the system mass (A) in agreement with Refs. [10,12,13,18,31,36]. Also, the EVF is higher with HMD EOS throughout the mass range compared to that with SMD EOS. This is due to the fact that higher density is achieved with SMD EOS than with HMD EOS, leading to higher repulsion (because of MDI) in the former, thus enhancing the flow and lowering the EVF. Also, the number of binary collisions is higher with SMD EOS (compared to that with HMD EOS), thus resulting in stronger repulsion among nucleons. Moreover, the role of nuclear compressibility increases with system size as predicted in Ref. [11], thus resulting in slightly weaker mass dependence of the EVF ($\tau = 0.27$) with HMD EOS compared to that with SMD EOS ($\tau = 0.33$).

In Fig. 3(c), we display the EVF as a function of system mass for soft and hard EOS. From the figure, one notices similar mass dependence with slightly different power-law factors. The absence of MDI enhances the EVF of lighter systems drastically; on the other hand, because of lower energies involved in the case of heavier systems, MDI do not

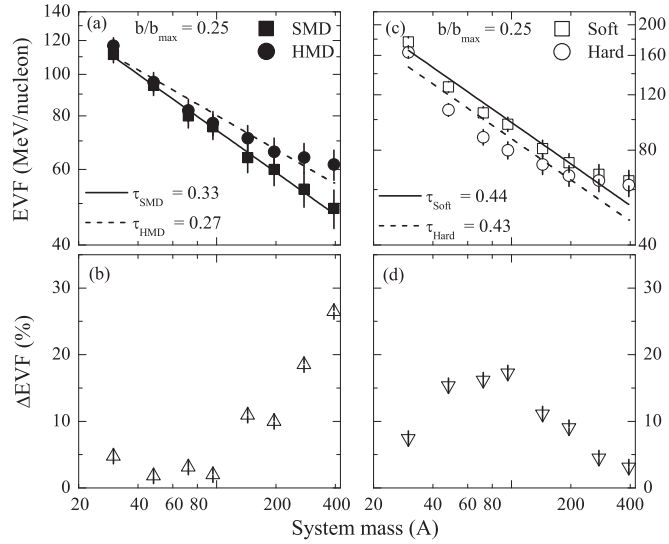

FIG. 3. Upper panels: The EVF as a function of system mass (A) for central collisions. Left- and right-hand panels correspond to the calculations with and without momentum dependence of the mean field. Lines represent the power-law fit $\propto A^{-\tau}$. Different symbols correspond to different EOS as explained in the text. Lower panels: The percentage change in the EVF [ΔEVF (%)] as a function of the system mass due to different EOS.

alter the EVF much in the latter and, thus, mass dependence becomes slightly stronger for static EOS. We also notice that the EVF is higher with soft EOS compared to that with hard EOS throughout the mass range as reported in Ref. [36], which is contrary to the earlier observations made in Fig. 3(a), where a HMD EOS leads to higher EVF compared to SMD EOS. This may happen because of the repulsive nature of the hard EOS compared to the soft EOS that enhances the directed transverse momentum imparted to nucleons. The power-law factor (τ) now becomes 0.44 and 0.43 for soft and hard EOS, respectively. It is worth mentioning that similar behavior of the nuclear EOS and its momentum dependence is also observed when the EVF are calculated for the systems whose experimental measurements (of EVF) are also available, but as stated earlier the power-law behavior is not absolute because of the varying colliding geometry, isospin content, and mass asymmetry of the reacting partners (results not shown here).

In Figs. 3(b) and 3(d), we display the percentage change in the EVF [ΔEVF (%)] as a function of total mass for hard and soft EOS, with and without MDI, respectively. The percentage change in the EVF is given by

$$\Delta\mathrm{EVF}(\%) = \left|\frac{\mathrm{EVF}^{\mathrm{H/HMD}} - \mathrm{EVF}^{\mathrm{S/SMD}}}{\mathrm{EVF}^{\mathrm{S/SMD}}}\right| \times 100. \qquad (2)$$

From Fig. 3(b), we find that when MDI are included, ΔEVF (%) increases with the system size, i.e., different nuclear compressibilities show greater sensitivity for the reactions involving heavier masses. It is well known that the time zone for which density remains substantially high increases with the mass of the system. Therefore, heavier systems can feel the compressional effects (due to different equations of state) to a greater extent compared to lighter ones. Also, a higher

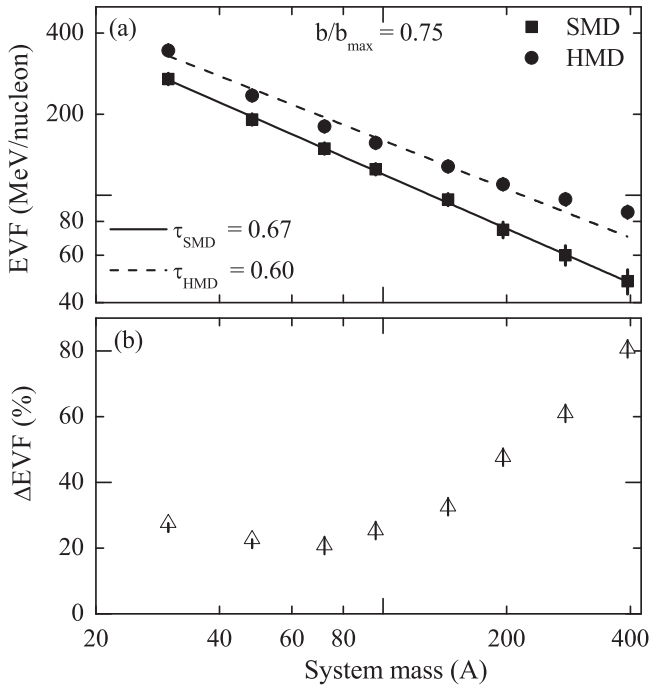

FIG. 4. Same as Fig. 3, but for the peripheral collisions with MDI only.

number of participating nucleons in heavier systems leads to significantly different binary *nn* collisions with soft and hard EOS that can also alter the directed transverse momentum. On the other hand, the number of collisions is almost insensitive to the nuclear compressibility in the case of reactions of lighter colliding nuclei. Therefore, both effects together lead to an enhanced net effect of nuclear compressibility in heavier masses.

Figure 3(d) displays ΔEVF (%) for static EOS. The behavior is contrary to that observed in Fig. 3(b); i.e., ΔEVF (%) now decreases with increases in the system mass. Now medium masses show greater sensitivity to EOS compared to heavier ones. This may happen due to the fact that lower densities are achieved as we move towards heavier masses (because of the lower EVF in heavier nuclei) and both EOS behave nearly the same at lower densities. It should also be noted that in the absence of MDI, the number of binary *nn* collisions increases drastically. Thus the sensitivity of collisions to nuclear EOS (as observed with MDI) starts disappearing as one moves from lighter to heavier colliding nuclei and therefore both EOS lead to almost the same directed transverse momentum in the reactions of heavier colliding nuclei.

Next, we investigate the role of EOS at peripheral collisions. In Fig. 4(a), we display the system size dependence of EVF with SMD and HMD EOS. The symbols have the same meaning as those in Fig. 3. From the figure we find that HMD EOS lead to higher EVF throughout the mass range because of the less directed transverse momentum with HMD EOS (as discussed earlier for peripheral collisions). We also notice that for peripheral collisions, the EVF follows a stronger system mass dependence, with a power-law factor close to 0.6. Such stronger mass dependence in peripheral collisions has also been reported in various earlier studies [23,24]. The EVF for lighter systems rises drastically when we go from central to peripheral collisions. This happens because a decreased participant zone at peripheral collisions demands higher incident energy to overcome the effects of the attractive mean field. On the other hand, increasing the role of Coulomb repulsion (in peripheral colliding geometries) in heavier colliding nuclei counteracts the attractive mean field and weakens the impact parameter dependence of the EVF and it remains nearly insensitive to the colliding geometry [12]. This mass-sensitive behavior of the EVF towards the colliding geometry leads to a steeper mass dependence. Figure 4(b) displays the percentage change in EVF with HMD and SMD EOS. We find that the ΔEVF (%) increases with system size as reported in central collisions. It is worth mentioning that the difference in the EVF due to both EOS is much more pronounced in peripheral collisions than in central ones because the ΔEVF (%) varies between 5% and 25% for central collisions whereas it increases to between 25% and 80% in peripheral geometries. It may be due to the delayed time zone of the reactions in peripheral collisions and thus compressional effects can be felt for longer duration and the effect of different EOS is enhanced. Therefore, peripheral collisions are better candidates to pin down the behavior of nuclear compressibility compared to central ones.

IV. SUMMARY

In summary, using a IQMD model, we studied the impact parameter dependence of the EVF for various reactions for which experimental measurements are available. Our calculations using SMD EOS along with a 20% reduced *nn* cross section reproduced the experimental trends for all the reactions. We also studied the role of different nuclear compressibilities (nuclear EOS) with and without momentum dependence of the mean field on the mass dependence of the EVF for the whole mass range between 30 and 394 units. The sensitivity of the EVF towards different static EOS (hard and soft EOS) is greater in the case of lighter colliding pairs, contrary to the calculations using MDI, where reactions of heavier nuclei showed more sensitivity.

ACKNOWLEDGMENTS

This work is supported by a grant from the Department of Science and Technology (DST), Government of India (Grant No. SR/FTP/PS-185/2012). The authors are also thankful to Professor Rajeev K. Puri for fruitful discussions.

[1] W. Scheid, H. Müller, and W. Greiner, Phys. Rev. Lett. **32**, 741 (1974); H. A. Gustafsson *et al.*, *ibid.* **52**, 1590 (1984).

[2] G. F. Bertsch, W. G. Lynch, and M. B. Tsang, Phys. Lett. B **189**, 384 (1987).

[3] J. Jaenicke *et al.*, Nucl. Phys. A **536**, 201 (1992).
[4] P. Danielewicz, Nucl. Phys. A **685**, 368 (2001); P. Danielewicz *et al.*, Phys. Rev. C **38**, 120 (1988); P. Danielewicz, R. Lacey, and W. G. Lynch, Science **298**, 1592 (2002).
[5] Q. Pan and P. Danielewicz, Phys. Rev. Lett. **70**, 2062 (1993).
[6] S. Kumar, S. Kumar, and R. K. Puri, Phys. Rev. C **78**, 064602 (2008); D. Sisan *et al.*, *ibid.* **63**, 027602 (2001) ; Y. K. Vermani, S. Goyal, and R. K. Puri, *ibid.* **79**, 064613 (2009); Y. K. Vermani and R. K. Puri, J. Phys. G: Nucl. Part. Phys. **36**, 105103 (2009); S. Kaur and R. K. Puri, Phys. Rev. C **87**, 014620 (2013).
[7] V. Kaur, S. Kumar, and R. K. Puri, Nucl. Phys. A **861**, 37 (2011); F. Fu *et al.*, Phys. Lett. B **666**, 359 (2008); B. Hong *et al.*, Phys. Rev. C **57**, 244 (1998); G. Q. Zhang *et al.*, *ibid.* **84**, 034612 (2011).
[8] C. Sturm *et al.*, Phys. Rev. Lett. **86**, 39 (2001); C. Hartnack, J. Jaenicke, L. Shen, H. Stöcker, and J. Aichelin, Nucl. Phys. A **580**, 643 (1994); C. Fuchs, Prog. Part. Nucl. Phys. **56**, 1 (2006); C. Hartnack *et al.*, Phys. Rep. **510**, 119 (2012).
[9] D. Krofcheck *et al.*, Phys. Rev. Lett. **63**, 2028 (1989); Phys. Rev. C **43**, 350 (1991); **46**, 1416 (1992).
[10] G. D. Westfall *et al.*, Phys. Rev. Lett. **71**, 1986 (1993).
[11] H. Y. Zhang *et al.*, Eur. Phys. J. A **15**, 399 (2002).
[12] D. J. Magestro, W. Bauer, and G. D. Westfall, Phys. Rev. C **62**, 041603(R) (2000).
[13] D. Klakow, G. Welke, and W. Bauer, Phys. Rev. C **48**, 1982 (1993).
[14] H. Zhou, Z. Li, and Y. Zhuo, Phys. Lett. B **318**, 19 (1993); Phys. Rev. C **50**, R2664 (1994).
[15] H. M. Xu, Phys. Rev. Lett. **67**, 2769 (1991); Phys. Rev. C **46**, R389 (1992).
[16] Z. Y. He *et al.*, Nucl. Phys. A **598**, 248 (1996).
[17] A. D. Sood and R. K. Puri, Eur. Phys. J. A **30**, 571 (2006).
[18] A. D. Sood, R. K. Puri, and J. Aichelin, Phys. Lett. B **594**, 260 (2004); A. D. Sood and R. K. Puri, Phys. Rev. C **69**, 054612 (2004).
[19] R. Pak *et al.*, Phys. Rev. C **54**, 2457 (1996); **53**, R1469 (1996).
[20] G. D. Westfall, Nucl. Phys. A **681**, 343 (2001).
[21] R. Pak *et al.*, Phys. Rev. Lett. **78**, 1022 (1997); **78**, 1026 (1997).
[22] S. Gautam *et al.*, J. Phys. G: Nucl. Part. Phys. **37**, 085102 (2010).
[23] S. Kumar, M. K. Sharma, R. K. Puri, K. P. Singh, and I. M. Govil, Phys. Rev. C **58**, 3494 (1998); R. Chugh and R. K. Puri, *ibid.* **82**, 014603 (2010); Int. J. Mod. Phys. E **19**, 2009 (2010).
[24] S. Gautam, A. D. Sood, R. K. Puri, and J. Aichelin, Phys. Rev. C **83**, 014603 (2011).
[25] S. Goyal and R. K. Puri, Nucl. Phys. A **853**, 164 (2011); S. Goyal, Eur. Phys. J. A **49**, 153 (2013).
[26] J. Łukasik *et al.*, Phys. Lett. B **608**, 223 (2005).
[27] J. C. Angélique *et al.*, Nucl. Phys. A **614**, 261 (1997); **583**, 543 (1995).
[28] A. Buta *et al.*, Nucl. Phys. A **584**, 397 (1995).
[29] J. P. Sullivan *et al.*, Phys. Lett. B **249**, 8 (1990).
[30] D. Cussol *et al.*, Phys. Rev. C **65**, 044604 (2002).
[31] D. J. Magestro *et al.*, Phys. Rev. C **61**, 021602(R) (2000).
[32] S. Soff, S. A. Bass, C. Hartnack, H. Stocker, and W. Greiner, Phys. Rev. C **51**, 3320 (1995).
[33] C. Liewen, Z. Fengshou, and J. Genming, Phys. Rev. C **58**, 2283 (1998).
[34] M. Kaur, V. Kaur, and S. Kumar, Phys. Rev. C **88**, 054620 (2013).
[35] R. Bansal, S. Gautam, and R. K. Puri, J. Phys. G: Nucl. Part. Phys. **41**, 035103 (2014).
[36] A. D. Sood and R. K. Puri, Phys. Rev. C **73**, 067602 (2006).
[37] C. Hartnack *et al.*, Eur. Phys. J. A **1**, 151 (1998); S. Kumar, S. Kumar, and R. K. Puri, Phys. Rev. C **81**, 014601 (2010); **81**, 014611 (2010).
[38] S. Gautam, A. D. Sood, R. K. Puri, and J. Aichelin, Phys. Rev. C **83**, 034606 (2011).
[39] Rajni, S. Kumar and R. K. Puri, Nucl. Phys. A **875**, 173 (2012); A. Jain, S. Kumar, and R. K. Puri, Phys. Rev. C **85**, 064608 (2012); R. Bansal, S. Gautam, R. K. Puri, and J. Aichelin, *ibid.* **87**, 061602(R) (2013).
[40] N. Bastid *et al.*, Phys. Rev. C **72**, 011901(R) (2005); F. Rami *et al.*, Nucl. Phys. A **646**, 367 (1999); W. Reisdorf *et al.*, *ibid.* **876**, 1 (2012).
[41] Y. Zhang, Z. Li, and P. Danielewicz, Phys. Rev. C **75**, 034615 (2007); L. W. Chen and C. M. Ko, Phys. Lett. B **634**, 205 (2006); Y. Zhang, P. Danielewicz, M. Famiano, Z. Li, W. G. Lynch, and M. B. Tsang, *ibid.* **664**, 145 (2008).
[42] V. Ramillien *et al.*, Nucl. Phys. A **587**, 802 (1995); P. Crochet *et al.*, *ibid.* **627**, 522 (1997); P. Danielewicz, *ibid.* **661**, 82 (1999); S. Kumar and R. K. Puri, Phys. Rev. C **60**, 054607 (1999).
[43] B. Blättel, V. Koch, A. Lang, K. Weber, W. Cassing, and U. Mosel, Phys. Rev. C **43**, 2728 (1991).